

CONVECTION AND HEAT TRANSFER IN LIQUID UNDER LOW GRAVITY CONDITIONS AND THERMOCAPILLARY EFFECTS.

Gadiyak G. V., Cheblakova E. A.

Institute of Computational Technologies,
Siberian Division of the Russian Academy of Sciences,
Lavrentyev av. 6, Novosibirsk, 630090, Russia

E-mail address: lena@net.ict.nsc.ru

Fax number: (3832) 341342

Fone number: (3832) 342280

Abstract

The two-dimensional flow of viscous incompressible liquid in a square cavity with a free boundary and differentially heated vertical sides is considered in the present work. The influence of gravitational and thermocapillary convection on temperature and velocity fields is studied in large range of dimensionless parameters and similarity criteria using equations in a Boussinesq approximation. Limiting cases of dimensionless parameters are analyzed numerically.

Introduction

It is known that in the nonuniformly heated fluid motion appears. Without free boundaries it appears due to thermal (gravitational) convection. In the nonuniformly heated liquid with a free boundary there arises thermocapillary convection [1], [2]. Under the low gravity condition it is necessary to take into account both of these processes. It is interesting to analyze the influence of these factors on heat fluxes and velocity fields formation under the non-gravity condition and with an increase in gravity.

We will consider a plane stationary convectional system with a side heating. Such a formulation of the problem is realized in practice, for example, in crystal growth

equipment, various energy plants [2], [3]. That is why the knowledge of flow and heat fluxes structure in the large dimensionless parameters range (Rayleigh Ra , Prandtl Pr and Marangoni Ma numbers) is of scientific and practical interest.

Model

The stream function - vorticity ($\psi-\omega$) formulation of the problem was used. For plane geometry initial non-dimensional stationary convection equations in a Boussinesq approximation under the non-gravity condition are the following [4]:

$$\frac{\partial}{\partial x}(u\omega) + \frac{\partial}{\partial y}(v\omega) = \frac{Pr}{Ma} \nabla^2 \omega, \quad (1)$$

$$\nabla^2 \psi = \omega, \quad (2)$$

$$\frac{\partial}{\partial x}(uT) + \frac{\partial}{\partial y}(vT) = \frac{1}{Ma} \nabla^2 T. \quad (3)$$

where $u = \frac{\partial \psi}{\partial y}$, $v = -\frac{\partial \psi}{\partial x}$, $\omega = \frac{\partial u}{\partial y} - \frac{\partial v}{\partial x}$.

The problem is characterized by the following parameters: the Marangoni number $Ma = \frac{\Delta T \sigma_T L}{\mu a}$ and the Prandtl number $Pr = \frac{\mu}{\rho a}$. Here $\Delta T = T_H - T_C$, T_H is the hot wall temperature, T_C is the cold wall temperature, σ_T denotes the temperature coefficient of surface tension, L stands for the characteristic length (the side of a square cavity), μ is the dynamic viscosity, ρ designates the density, a is the thermal diffusivity.

Calculations with various Prandtl and Marangoni numbers were carried out. Two limiting cases were also considered: $Ma \rightarrow 0$ and $Pr \rightarrow \infty$. If the Marangoni number tends to zero (i.e. surface tension force is equal to zero) then the set of Eqs. (1 – 3) is modified as follows:

$$\nabla^2 \omega = 0, \quad (4)$$

$$\nabla^2 \psi = \omega, \quad (5)$$

$$\nabla^2 T = 0. \quad (6)$$

If the Prandtl number tends to infinity (that is the case of the strongly viscous fluid) then the set of Eqs. (1 – 3) is developed as follows:

$$\nabla^2 \omega = 0, \quad (7)$$

$$\nabla^2 \psi = \omega, \quad (8)$$

$$\frac{\partial}{\partial x}(uT) + \frac{\partial}{\partial y}(vT) = \frac{1}{Ma} \nabla^2 T. \quad (9)$$

If the force of gravity g is not equal to 0, initial stationary non-dimensional equations of thermal convection in a Boussinesq approximation in the uniform gravitational field in $(\psi - \omega)$ variables are then [4]:

$$\frac{\partial}{\partial x}(u\omega) + \frac{\partial}{\partial y}(v\omega) = \frac{Pr}{Ma} \nabla^2 \omega - \frac{Ra \cdot Pr}{Ma^2} \frac{\partial T}{\partial x}, \quad (10)$$

$$\nabla^2 \psi = \omega, \quad (11)$$

$$\frac{\partial}{\partial x}(uT) + \frac{\partial}{\partial y}(vT) = \frac{1}{Ma} \nabla^2 T. \quad (12)$$

Here $Ra = \frac{\beta \rho g L^3 (T_H - T_C)}{a \mu}$ is the Rayleigh number, $\beta = -\frac{1}{\rho} \frac{\partial \rho}{\partial T}$ denotes the volumetric coefficient of thermal expansion.

In the present work the following boundary conditions are considered. The vertical sides are at temperatures $T = T_H = 0,5$ ("hot" wall) and $T = T_C = -0,5$ ("cold" wall). The lower horizontal wall and the free surface $y = 1$ are insulated. Both velocity components are zero on the walls. On the free surface the component $\mu \frac{\partial u}{\partial y}$ of the viscous tension tensor is equal to the tangential force acting on the surface $-\sigma_T \frac{\partial T}{\partial x}$, and vertical velocity v is equal to zero. Thus the boundary conditions for the considered equations can be written in the following way:

$$\psi = \frac{\partial \psi}{\partial x} = 0, \quad T = T_H = 0,5 \quad \text{at } x = 0,$$

$$\psi = \frac{\partial \psi}{\partial x} = 0, \quad T = T_C = -0,5 \quad \text{at } x = 1,$$

$$\psi = \frac{\partial \psi}{\partial y} = 0, \quad \frac{\partial T}{\partial y} = 0 \quad \text{at } y = 0,$$

$$\psi = 0, \quad \frac{\partial^2 \psi}{\partial y^2} = -\frac{\partial T}{\partial x}, \quad \frac{\partial T}{\partial y} = 0 \quad \text{at } y = 1.$$

The case of the surface tension force equal to zero was also considered. This corresponds to the system (4 – 6) with the boundary condition $\frac{\partial u}{\partial y}|_{y=1} = 0$:

$$\psi = 0, \quad \frac{\partial^2 \psi}{\partial y^2} = 0 \quad \text{at } y = 1.$$

Method of solution

Formulation of the problem (1 – 3), as many other problems of viscous incompressible fluid in (ψ, ω) variables has the following difficulty. Boundary conditions on the walls are determined only for the stream function, and not for the vorticity, which is defined

only inside the domain according to the Eq. (2). To overcome this difficulty various approaches are used, for example, approximate boundary conditions for vorticity. In the present work we use the Toma condition for ω on the wall [5]:

$$\omega_k = \frac{2(\psi_{k+1} - \psi_k)}{\Delta h^2} + O(\Delta h). \quad (13)$$

Here Δh denotes the mesh size, ψ_k is the value of the stream function in the boundary node k , ψ_{k+1} is the value of ψ in the node $k + 1$ nearest to the wall.

Calculations were also performed with the second order boundary condition for ω , namely, Woods condition. Computational results with these different conditions are almost the same. However, the use of the approximate boundary conditions for vorticity on the wall for the Eqs. (1 – 3) at high Marangoni numbers and on fine meshes leads to the considerable slowing-down of the convergence. That is why we also used the boundary conditions calculation method [6], which allowed us to improve the convergence in 2 – 4 times, and in some cases on the order in comparison with the use of the Toma formula.

Idea of this method is to determine the boundary condition for vorticity inside the main domain, where ω is defined according to (2). Equation for ω (1) is solved in the auxiliary domain. The solid boundaries of this domain are displaced on the mesh size into the cavity from the solid boundaries of the main domain. The free surface $y = 1$ is common for these domains. On the free surface vorticity is determined as follows:

$$\omega|_{y=1} = \frac{\partial u}{\partial y}|_{y=1} = -\frac{\partial T}{\partial x}|_{y=1}.$$

Stream function and temperature equations are solved in the main domain. There are two boundary conditions for the stream function. The condition $\psi_0 = 0$ is used to solve equation for ψ . The obtained stream function field does not satisfy the gradient condition $(\frac{\partial \psi}{\partial n})|_{x=0, x=1, y=0} = 0$ yet. Therefore, the values of ψ on the boundary of the auxiliary domain are corrected with the help of the difference analog of this condition [6]. Using a three-point approximation of the second order for the derivative $(\frac{\partial \psi}{\partial n})|_{x=0, x=1, y=0}$ we will obtain:

$$\text{at } x = 0 \quad \psi_{2j} = \frac{1}{4}\bar{\psi}_{3j}, \quad j = 2, \dots, m - 1;$$

$$\text{at } x = 1 \quad \psi_{n-1j} = \frac{1}{4}\bar{\psi}_{n-2j}, \quad j = 2, \dots, m - 1;$$

$$\text{at } y = 0 \quad \psi_{i2} = \frac{1}{4}\bar{\psi}_{i3}, \quad i = 2, \dots, n - 1.$$

When approximating Eqs. (1, 3) and (10, 12) for temperature and vorticity exponential fitting discretization (or scheme of integral identities) was used [7], [8]. It allowed us to obtain a higher precision in comparison with the usual approximations. As a result, a five-point algebraic system was carried out. Equations for ω and T do not satisfy the diagonal dominance condition. It is known that without this condition, many effective methods fail to converge or converge very slowly. In the present work modification of Buleev's method [9] and a splitting method [10] are used. They enable to find a solution of the system without a diagonal dominance property. Buleev's method modification converges faster than the splitting method when the stream function and the temperature equations are solved. But for the vorticity equation with high Marangoni numbers ($Ma > 10^2$) Buleev's method does not converge to the necessary precision (namely, $1.e - 7$). Thus the equation for ω was solved by splitting which enables to obtain the prescribed precision.

To improve convergence the damping operation for vorticity was used. It is determined by the following recurrent relation:

$$\omega_d^{n+1} = \theta\omega^{n+1} + (1 - \theta)\omega_d^n,$$

where θ stands for the damping parameter, ω_d^n is the damped value of vorticity from the n iteration, ω^{n+1} denotes the value of ω from the $n + 1$ iteration.

During numerical experiments for a 61×61 mesh the damping parameter θ was about 0,002.

Main results and their analysis

We use rectangular non-uniform thickening to the boundary of the 21×21 , 41×41 and 61×61 area grids. Calculations were performed at the Marangoni numbers from 10^{-3} to 10^4 , the Prandtl numbers from 1 to 100 and the Rayleigh numbers from 0 to 10^6 . Two limiting cases: $Ma \rightarrow 0$ and $Pr \rightarrow \infty$ were also considered. Results are presented in Figures (1-10) and in Tables I and II on the 61×61 mesh. Results at the Marangoni number $Ma = 10^4$ are not very reliable as the calculating scheme converges badly at this value of dimensionless parameter.

Figure 1 shows the influence of surface tension force on the temperature field under the non-gravity condition ($Ra = 0$). If the Marangoni number $Ma = 0$, i.e.

the surface tension force is equal to zero (Fig.1a), there is no convection, and the fluid rests. With an increase in the Marangoni number the convective mixing enhances, and at $Ma = 10^4$ the flow becomes vortical. One can see from Figures 1b, 1c, 1d, that the greater Ma , the stronger the contour maps deflect and are pressed to the hot and cold walls. Near these walls temperature boundary layers appear. The boundary layer near the hot wall is wider than near the cold. One characteristic property of the picture is the condensation of contour maps to the upper right corner of the cavity, to the region near the free surface and the cold wall. In the center of the domain a vortex is formed. Contour maps on Figure 1 correspond to the Prandtl number $Pr = 1$. Figure 2 shows temperature contour maps at $Pr = \infty$ (that is the case of the strongly viscous fluid, Eqs. (7 – 9)). Behavior near the free surface $y = 1$ is different for the corresponding contour maps of Figures 1 and 2. In the case of the strongly viscous fluid contour maps come normally to the free surface and remain undeflected near it longer than in the case of $Pr = 1$. The explanation is that it is more difficult for the surface tension force to mix more viscous fluid. From the comparison of contour maps at $Ma = 10^4$ (Figures 1d and 2c) one can see that at $Pr = 1$ a vortex region is larger and extend almost over the entire domain. At $Pr = \infty$ the vortex is situated closer to the free surface, convective flow in the entire domain is weaker. Thus the more viscosity of the fluid, the weaker convection there at the same surface tension force.

Figure 3 presents the influence of the gravity (Ra) on the temperature field. Analyzing the results, we can say that with the increase in Rayleigh number the whole picture of the flow becomes more complex, convection mixing of the fluid intensifies, the vortical structure of the stream and narrow boundary layers with the sharp temperature difference across the boundary layer near the hot and cold walls appear. Comparison of corresponding contour maps of Figures 1 and 3 shows that the surface tension force tends to form a vortex in the center of the domain and to condense the contour maps to the upper part of the cold wall; whereas the force of gravity tends to form a vortex closer to the boundary of the cavity, remaining its center without a vortex, and to condense the contour maps to the vertical walls. At $Ra = 10^6$ two narrow boundary layers near the vertical sides of the width $\approx 0,07$ each, with horizontal temperature gradient are generated. In the remaining part of the calculation

Ra	$max v $	x	y
10^2	11,871	0,6776	1
10^3	13,639	0,6776	1
10^4	26,626	0,5	1
10^5	73,827	0,3225	1
10^6	192,88	0,0541	0,5969

Table 1: Dependence of the maximum value of velocity module and its location on the Rayleigh number.

domain of the width $\approx 0,85$ the contour maps are located at a greater distance and the temperature gradient points vertically upwards. Such behavior of the temperature contour maps influences the stream function field. One can see from Figure 4d for the ψ contour maps ($Ra = 10^6$) that near the vertical walls contour maps condense, and two narrow boundary layers with the sharp difference of stream function values across the boundary layer are formed. In the remaining part of the calculation domain the contour maps are located at a greater distance. At $Ra = 10^5$ (Fig.4c) the secondary flows are formed in the center of the domain.

Table I shows an increase in the maximum value of velocity module $\sqrt{u^2 + v^2}$ and the change in its location with an increase in the Rayleigh number. At $Ra \leq 10^5$ this maximum is situated on the free surface, and the greater Ra , the closer the maximum to the hot wall. At $Ra = 10^6$ the maximum value of $\sqrt{u^2 + v^2}$ is located close to the center of the hot wall.

Dependence of the maximum value location of $\sqrt{u^2 + v^2}$ on the Marangoni number was built (Fig.5). For all considered Ma numbers the maximum value of velocity module is situated on the free surface. With an increase in Ma it moves to the upper right corner, the common point of the cold wall and the free surface. For a more viscous fluid this maximum is located closer to the hot wall for the same Marangoni numbers. It is evident that the surface tension force tends to move the vortex to the upper boundary of the cold wall, and it is more difficult to mix more viscous fluid. In the range of Ma from 10^3 to 10^4 some oscillation of the curve can be seen (Fig.5). It is connected with the more complex structure of the flow at the high

Marangoni numbers. A high precision is necessary for the calculation of the flow at the Marangoni numbers $Ma \geq 10^4$. Such precision could not be obtained with the help of the proposed scheme.

Figure 6 presents the contour maps of stream function at $Pr = 1$, $Ra = 0$ for various Marangoni numbers. With an increase in Ma the contour maps begin to come closer to the upper corners, and in the lower corners the secondary flows appear. With the increase in the Marangoni number the inner vortex domain increases, and the contour maps value module corresponding to this vortex decreases. The contour maps condense near the free surface.

Figure 7 shows ψ contour maps for the strongly viscous fluid at different Marangoni numbers. One can see from a comparison of Figures 6 and 7 that in more viscous fluid the convective flow in the entire calculation domain is weaker, vortex is located closer to the free surface and vortex's region is less; there are no secondary flows in the lower corners of the domain.

Let us compare Figures 6a ($Pr = 1$, $Ma = 10^2$, $Ra = 0$) and 4a ($Pr = 1$, $Ma = 10^2$, $Ra = 10^3$). With the appearance of the thermal gravitational convection the contour maps shape changes. The lower parts of the contour maps are located closer to the bottom of the domain, and contour maps tend to the lower corners. It is the result of the gravity force influence. The greater Ra , the stronger the influence of the gravity force in comparison with the surface tension force on the character of the flow. Thus at $Ra = 10^3$, $Ma = 10^2$ (Fig.4) the contour maps also tend to the upper right corner, i.e. the thermocapillary convection considerably influences the contour maps shape. With the further increase in Ra the gravitational convection becomes dominant. Beginning from $Ra = 10^5$ the secondary flows are formed. One of them tends to the upper left corner of the cavity, to the hot wall, another - to the lower right corner, to the cold wall (Fig.4b, 4c, 4d).

Calculations of the convection problem under the non-gravity condition with the surface tension force equal to zero (Eqs. (4 – 6) with the zero boundary condition $\frac{\partial u}{\partial y}|_{y=1} = 0$) were made. Here no forces operate on the fluid, there is no convection, and all profiles of stream function, velocities and vorticity at various sections of the calculation domain are almost zero. The temperature contour maps in this case are straight lines (Fig.1a). It means that the heat is transferred only by heat conduction.

Calculations of the convection problem without gravitation were also carried out with the following parameters: $Ma = 1; 0,1; 0,01; 0,001; Pr = 1$. With the decrease in the Marangoni number the stream function and velocity profiles tend monotonously to the zero values, to the profiles of the limiting case $Ma = 0$. The temperature contour maps also tend monotonously to the contour maps of the case $Ma = 0$ with the decrease in Ma .

Another limiting case: $Pr \rightarrow \infty$ for various Marangoni numbers (Eqs. (7 – 9)) under the non-gravity condition was also considered. Computational results show that for every Marangoni number between 0 and 10 the flow does not depend on the Prandtl number (at Pr between 1 and ∞). At $Ma = 10^2$ and Pr from 10 to ∞ the corresponding profiles of the flow agree (Fig.2a (temperature contour maps), Fig.7a (contour maps of ψ)), but differ from the flow profiles at the Prandtl number $Pr = 1$ (Fig.1b, 6a). A similar situation takes place at $Ma = 10^3$ (Fig.1c, 6b; 2b, 7b). At $Ma = 10^4$ and $Pr = 100, \infty$ the profiles are close to each other and differ from the flow profiles at $Pr = 10$.

For the heat balance control the average Nusselt numbers on the hot and cold walls and on the vertical mid-plane of the cavity were calculated. The local Nusselt number $Nu(x, y)$ at the point (x, y) and the average Nusselt number Nu_{x_0} on the section $x = x_0$ are determined as follows:

$$Nu(x, y) = Ma \cdot uT - \frac{\partial T}{\partial x},$$

$$Nu_{x_0} = \int_0^1 Nu(x_0, y) dy.$$

Table II shows the computational results of the convection problem in the cavity with a free surface and side heating under the non-gravity condition at $Pr = 1$ and various Marangoni numbers. Here $u(1/2, 1)$ is the value of u velocity at the mid-point of the free surface, $Nu_0, Nu_{1/2}, Nu_1$ designate the average Nusselt numbers on the sections $x = 0, x = 1/2, x = 1$ respectively. The obtained results were compared with [11]. In the work [11] a high accuracy scheme was used to solve Eqs. (1 – 3). One can see from the Table that the present work method allows us to obtain with acceptable precision the integral characteristics of heat-removing ($Nu_0, Nu_{1/2}, Nu_1$). However, the local characteristics ($Nu(0, 1), Nu(1, 1)$) are determined with essential

Ma	grid	$u(1/2,1)$	Nu_0	$Nu_{1/2}$	Nu_1	$Nu(0,1)$	$Nu(1,1)$
10^2	21×21	1,0326(-1)	1,1322	1,0999	1,0396	0,7972	1,7816
	41×41	1,0711(-1)	1,1010	1,0977	1,0867	0,7402	1,9874
	61×61	1,0671(-1)	1,0945	1,0953	1,0924	0,7313	1,9905
[11]	61×61	1,0869(-1)	1,0962	1,0962	1,0962	0,7301	2,028
10^3	21×21	5,2221(-2)	2,1800	1,9976	1,6900	1,3444	7,3224
	41×41	5,2032(-2)	1,9858	1,9742	1,8983	1,0268	10,6884
	61×61	5,1404(-2)	1,9437	1,9528	1,9297	0,9707	11,438
[11]	61×61	5,0018(-2)	1,9258	1,9258	1,9258	0,9550	11,75
10^4	21×21	2,7263(-2)	5,4250	3,9362	2,6086	5,1195	12,6693
	41×41	3,1541(-2)	4,5622	4,3744	4,1286	3,1227	38,5290
	61×61	3,1562(-2)	4,4459	4,4467	4,3524	2,5091	60,471
[11]	61×61	3,0381(-2)	4,3621	4,3621	4,3654	2,2334	77,09

Table 2: Computational results at $Pr=1$.

errors, particularly at $Ma = 10^4$.

Dependencies of the average Nusselt numbers on the Prandtl, Marangoni and Rayleigh numbers (Fig.8, 9 and 10 respectively) were also calculated. Fig.8 shows that the greater the Marangoni number for the same Prandtl number (i.e. the stronger thermocapillary convection), the stronger heat-removing. At Ma between 0 and 10^2 the heat-removing coefficient does not change with the increase in Pr . At $Ma = 10^3$; 10^4 and from $Pr = 10$ this coefficient takes some constant value, and every Marangoni number has its own value. Besides, at Ma between 10^3 and 10^4 an abrupt increase in the Nusselt number is observed, especially for the case $Pr = 1$. Probably, the reason for it lies in the appearance of a more complex structure of the flow and in the loss of it the stability [11], which lead to the sharp increase in heat-removing. Such an abrupt increase in heat-removing is also observed in Fig.9, which presents dependence of Nu on Ma for various Prandtl numbers. The Nusselt number increases with the growth of the Rayleigh number, which characterizes the intensity of the gravitational convection (Fig.10). At Ra between 10^4 and 10^6 abrupt increase

in the Nusselt number also occurs because of the appearance of a more complex flow structure. Figures 9, 10 present functions that are the parameter approximations of dependences of the Nusselt number on the hot wall on the Rayleigh number at Ra between 10^5 and 10^6 and on the Marangoni number at Ma between 10^3 and 10^4 . In figures these functions are showed by triangles ($\triangle \triangle \triangle$). They are the linear combinations of functions with the fitting coefficients as follows:

$g(Ma) = 1,481 + 7,15 \cdot 10^{-4} \cdot Ma - 3,277 \cdot 10^{-8} \cdot Ma^2$ - in the case of the Nusselt number on the Marangoni number dependence;

$g(Ra) = 4,122 + 9,507 \cdot 10^{-6} \cdot Ra - 4,296 \cdot 10^{-12} \cdot Ra^2$ - in the case of the Nusselt number on the Rayleigh number dependence.

Conclusions

1. The influence of gravitational and thermocapillary convection on the temperature and velocity fields has been studied. Computational results show that at $Ma \leq 10^2$ and beginning from $Ra = 10^4$ the gravitational convection becomes dominant.
2. With the increase in the gravity force the whole picture of the flow becomes more complex, convection mixing of the fluid intensifies, narrow boundary layers with the sharp temperature and velocity difference across the boundary layer close to the hot and cold walls appear. Beginning from $Ra = 10^5$ the secondary flows formation occurs.
3. In a more viscous fluid the convective flow in the entire calculation domain is weaker, vortexes are located closer to the free surface and vortexes region is less.
4. Two limiting cases: $Ma \rightarrow 0$ and $Pr \rightarrow \infty$ without gravitation were considered. Computational results show that with the decrease in the Marangoni number the flow profiles tend monotonously to the flow profiles of the case $Ma = 0$. Ranges of the dimensionless parameters where the flow does not change were also determined.
5. The parameter approximations of dependences of the Nusselt number on the hot wall on the Rayleigh number at Ra between 10^5 and 10^6 and on the Marangoni number at Ma between 10^3 and 10^4 were built.

Acknowledgements

The authors thank Berdnikov V. S., Gaponov V. A., Cheblakov G. B., Dvurechenskii A. V. for helpful discussions and encouragement. This work was supported by Russian Fund of Fundamental Researches under Grant N 96-01-00137.

References

- [1] Berdnikov, V. S. and Kirdyashkin, A. G., Structure of free-convective flows in the horizontal fluid layer under various boundary conditions. *Structure of wall boundary layer*, Novosibirsk, 1978, pp.5-45 (in Russian).
- [2] Avduevsky, V. S. and Polezhaev, V. I., *Hydrodynamics, heat and mass transfer during material processing*, Nauka, Moscow, 1990 (in Russian).
- [3] Dubovik, K. G., Nikitin, S. A. and Polezhaev, V. I., Hydrodynamical effects of temperature and concentrational stratification. *Problems of viscous flows*, Institute of theoretical and applied mechanics, Novosibirsk, 1981, pp.55-64 (in Russian).
- [4] Landau, L. D. and Lifshitz, E. M., *Fluid Mechanics*, Pergamon Press, Oxford, 1959.
- [5] Roache, P. J., *Computational fluid dynamics*, Hermosa Publishing, Albuquerque, NM, 1972.
- [6] Polezhaev, V. I. and Gryaznov, V. L., Boundary conditions calculation method for the Navier-Stokes equations in 'vorticity, stream function' variables. *Academy of Sciences reports*, 1974, **219**(2), 301-304 (in Russian).
- [7] Cheblakova, E. A. and Gadiyak, G. V., Convective flow in an upright enclosed square cavity: a comparison exercise. *International Journal of Computational Fluid Dynamics*, 1998, **10**(2), 139-149.
- [8] Marchuk, G. I., *Methods of numerical mathematics*, Springer, New York, 1982.
- [9] Schneider, G. E. and Zedan, M., A modified strongly implicit procedure for the numerical solution of field problems. *Numerical Heat Transfer*, 1981, **4**, 1-19.
- [10] Yanenko, N. N., *The method of fractional steps*, Springer-Verlag, New York/Berlin, 1971.

- [11] Berdnikov, V. S., Vinokurov, V. V. and Gaponov, V. A., Structure of thermal gravitational-capillary flows in Czochralski models. *III Siberian Congress on Industrial Applied Mathematics (INPRIM-98)*, 1998.
- [12] Samarskii, A. A. and Nikolaev, E. S., *Methods of solution of finite difference equations*, Nauka, Moscow, 1978 (in Russian).
- [13] Peyret, R. and Taylor, T. D., *Computational methods for fluid flow*, Springer, Berlin, 1983.
- [14] *Mathematical modelling of convective heat and mass transfer on the basis of Navier-Stokes equations*, Nauka, Moscow, 1987 (in Russian).

FIGURES

Fig.1. Contour maps of temperature T : $Pr = 1$, $Ra = 0$,
a - $Ma = 0$, b - $Ma = 10^2$, c - $Ma = 10^3$, d - $Ma = 10^4$.

Fig.2. Contour maps of temperature T : $Pr = \infty$, $Ra = 0$,
a - $Ma = 10^2$, b - $Ma = 10^3$, c - $Ma = 10^4$.

Fig.3. Contour maps of temperature T : $Pr = 1$, $Ma = 10^2$,
a - $Ra = 10^3$, b - $Ra = 10^4$, c - $Ra = 10^5$, d - $Ra = 10^6$.

Fig.4. Contour maps of stream function ψ : $Pr = 1$, $Ma = 10^2$,
a - $Ra = 10^3$, b - $Ra = 10^4$, c - $Ra = 10^5$, d - $Ra = 10^6$.

Fig.5. Maximum value location of the velocity module versus the Marangoni number
(— $Pr = 1$, - - $Pr = \infty$).

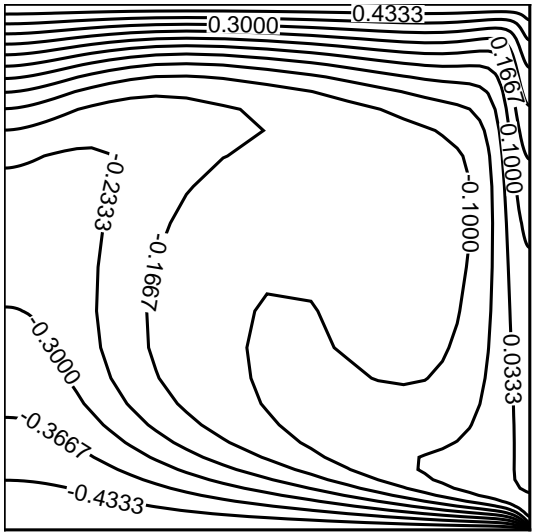
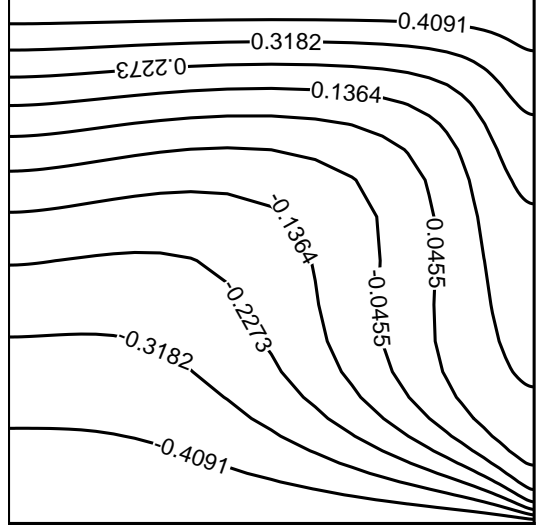
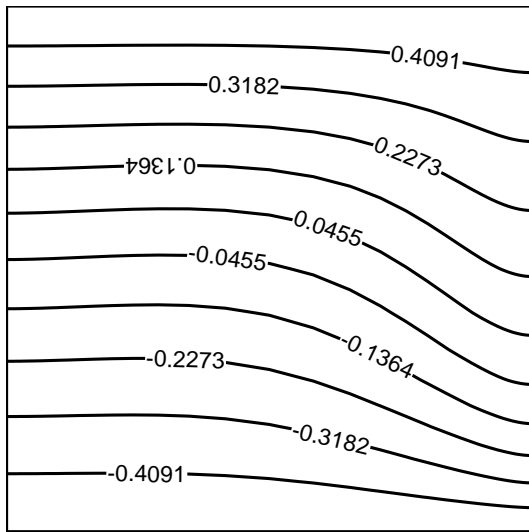
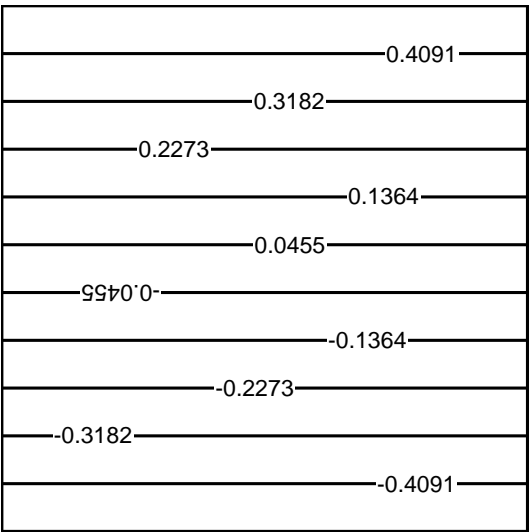
Fig.6. Contour maps of stream function ψ : $Pr = 1$, $Ra = 0$,
a - $Ma = 10^2$, b - $Ma = 10^3$, c - $Ma = 10^4$.

Fig.7. Contour maps of stream function ψ : $Pr = \infty$, $Ra = 0$,
a - $Ma = 10^2$, b - $Ma = 10^3$, c - $Ma = 10^4$.

Fig.8. Average Nusselt number on the hot wall versus the Prandtl number
(1 - $Ma = 0$, 2 - $Ma = 10^2$, 3 - $Ma = 10^3$, 4 - $Ma = 10^4$).

Fig.9. Average Nusselt number on the hot wall versus the Marangoni number
($g(Ma) = 1,481 + 7,15 \cdot 10^{-4} \cdot Ma - 3,277 \cdot 10^{-8} \cdot Ma^2$)
— $Pr = 1$, - - $Pr = \infty$, $\Delta \Delta g(Ma)$.

Fig.10. Average Nusselt numbers on the hot and cold walls versus the Rayleigh
number ($g(Ra) = 4,122 + 9,507 \cdot 10^{-6} \cdot Ra - 4,296 \cdot 10^{-12} \cdot Ra^2$)
— $Nu0$, - - $Nu1$, $\Delta \Delta g(Ra)$.

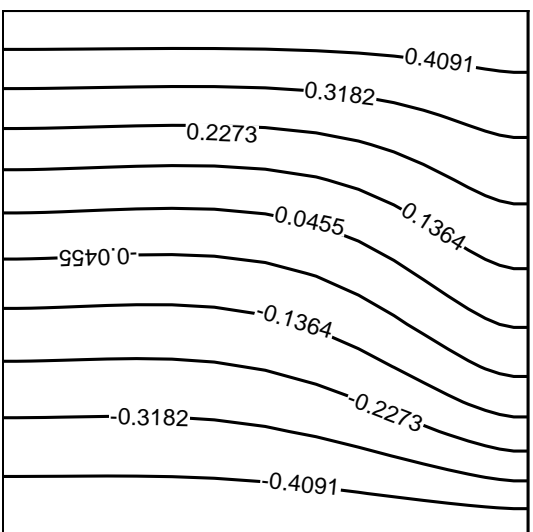


a

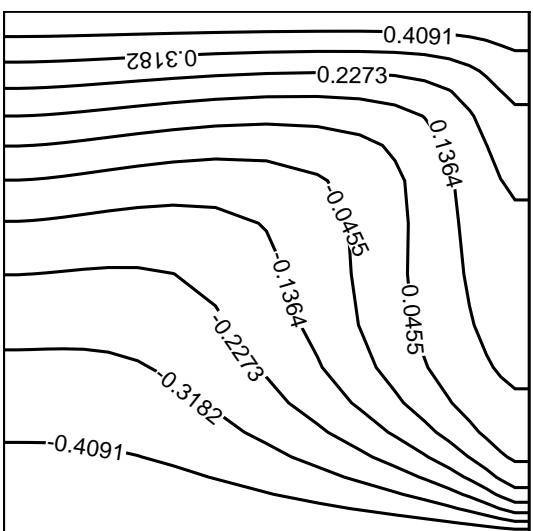
b

c

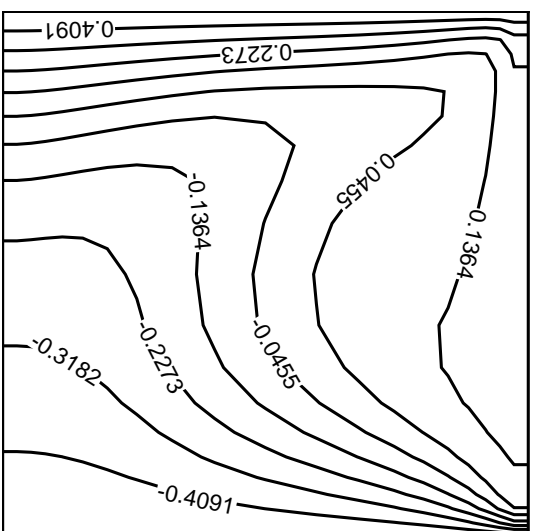
d



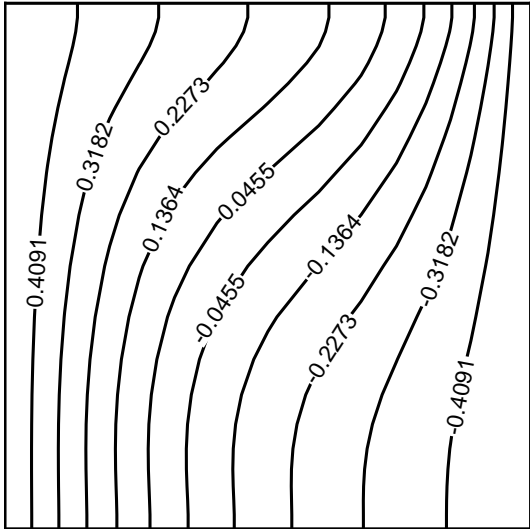
a



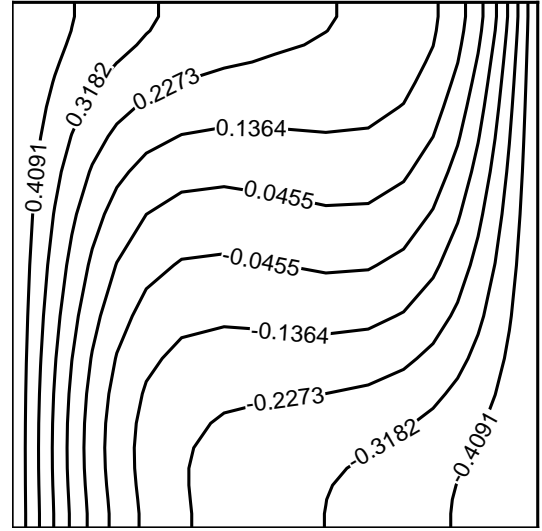
b



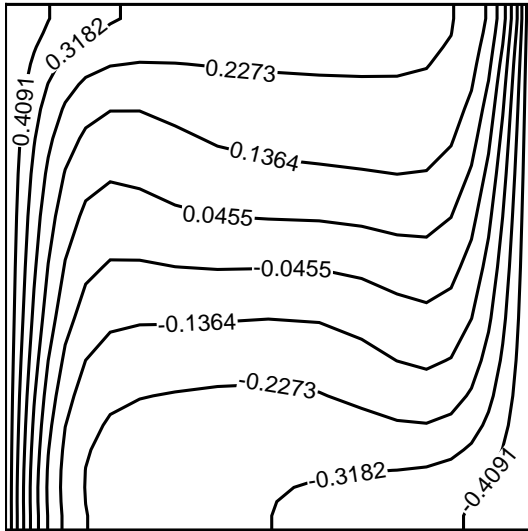
c



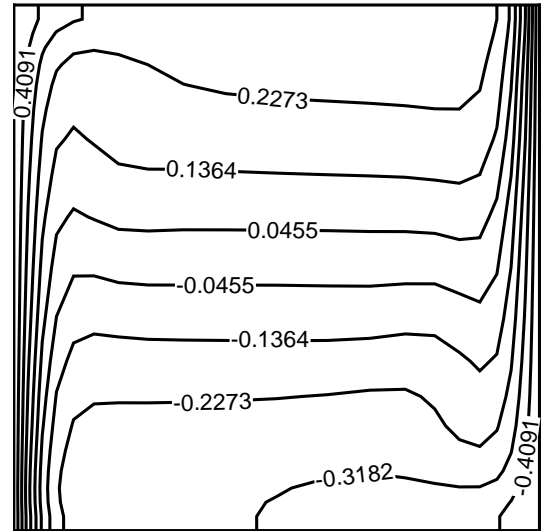
a



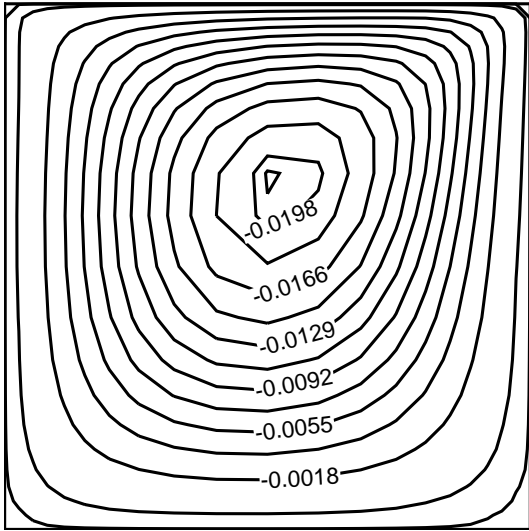
b



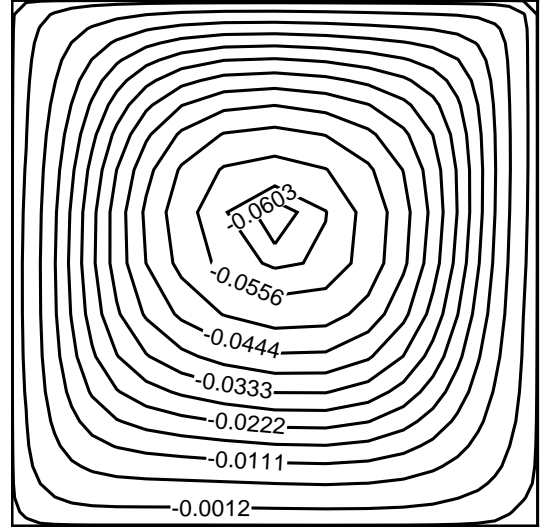
c



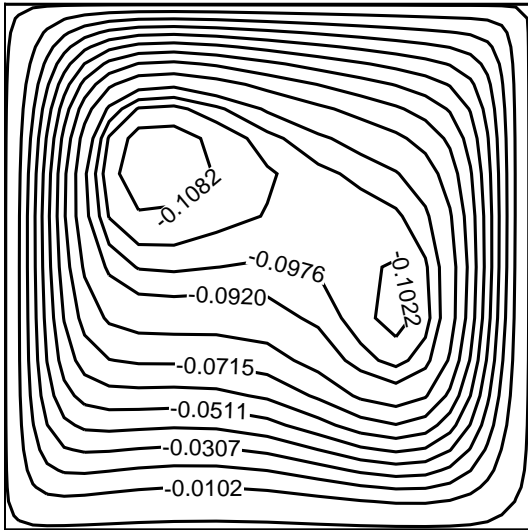
d



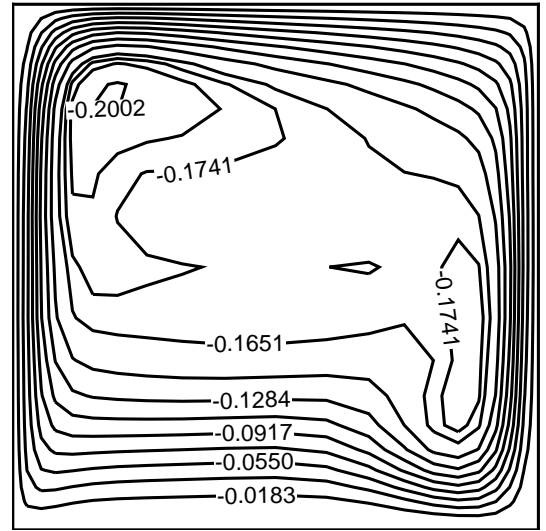
a



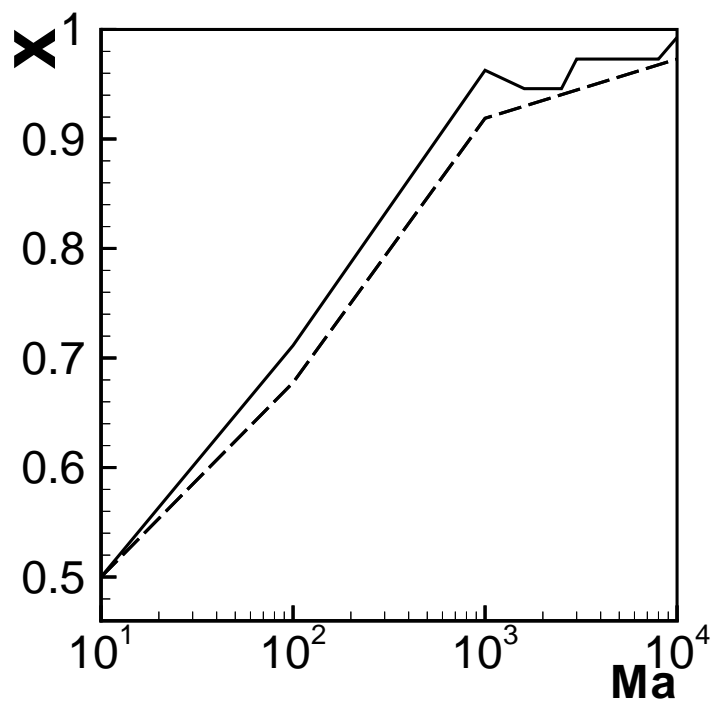
b

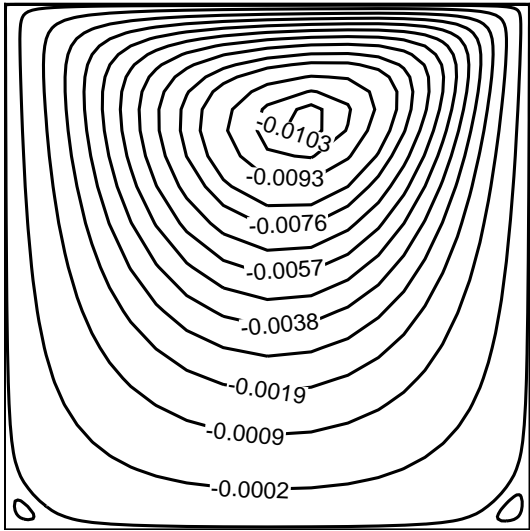


c

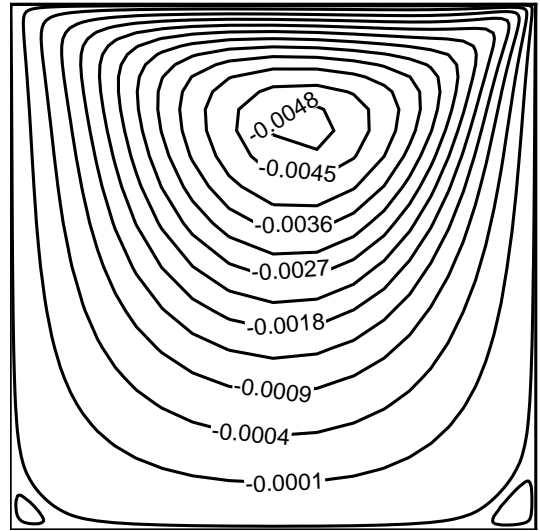


d

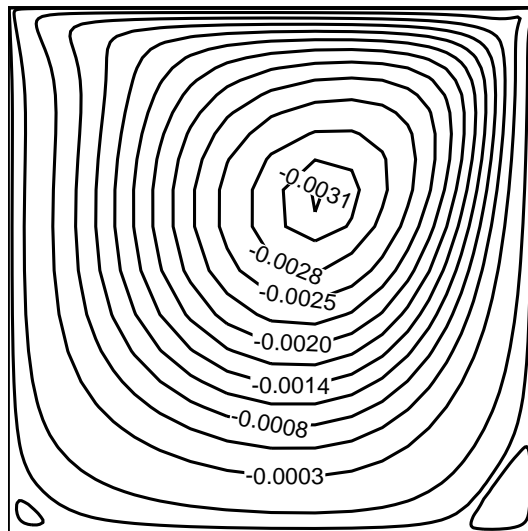




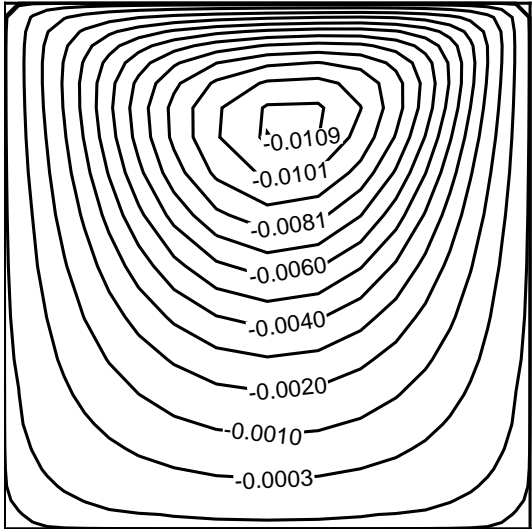
a



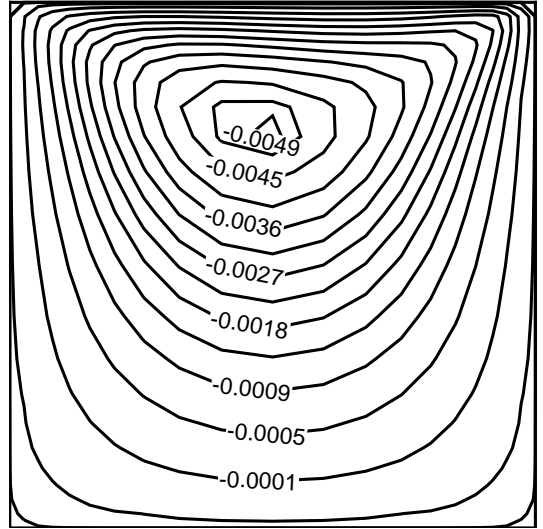
b



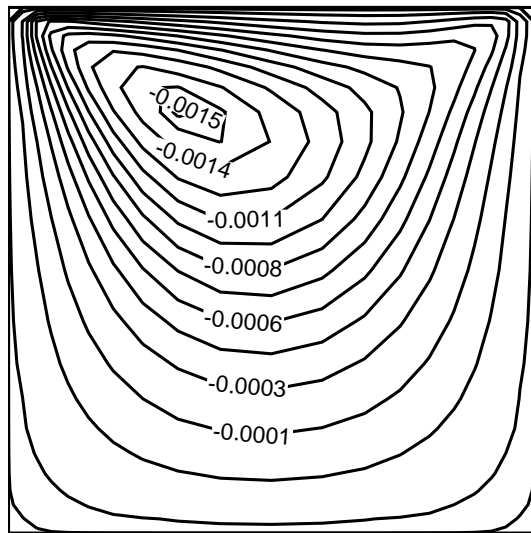
c



a



b



c

